

Measured Cosmological Mass Density in the WHIM: the Solution to the 'Missing Baryons' Problem

Fabrizio Nicastro^{a,*} Martin Elvis^a Fabrizio Fiore^c
Smita Mathur^b

^a*Harvard-Smithsonian Center for Astrophysics, 60 Garden Street, MS-83,
Cambridge, MA, 02138, U.S.A.*

^b*Astronomy Department, The Ohio State University, 43210, Columbus, OH,
U.S.A.*

^c*Osservatorio Astronomico di Roma, Monteporzio Catone, Italy*

Abstract

We review the current high-significance X-ray detections of Warm-Hot Intergalactic Medium (WHIM) filaments at $z > 0$ along the lines of sight to the two blazars Mrk 421 ($z = 0.03$) and 1ES 1028+511 ($z = 0.361$). For these WHIM filaments, we derive ionization corrections and, when possible, metallicity estimates. This allows us to obtain refined estimates of the number density of O VII WHIM systems down to the O VII column density sensitivity of our observations, and most importantly, a measurement of the cosmological mass density Ω_b^{WHIM} in the WHIM, at redshift $z < 0.361$. These estimates agree well with model predictions and with the total estimated amount of missing baryons in the local Universe, although errors are large, due to the still limited number of systems. We conclude discussing future observational strategies and mission designs for WHIM studies.

Key words: IGM, WHIM, Cosmological Mass Density

PACS:

1 'Missing Baryons' and the Warm-Hot Intergalactic Medium

The total number of baryons in the Universe, as inferred by both Big-Bang Nucleosynthesis (BBN) compared with observations of light element ratios (Kirk-

* F. Nicastro

Email address: fnicastro@cfa.harvard.edu (Fabrizio Nicastro).

man et al., 2003) and Cosmic Microwave Background (CMB) anisotropies (Bennett et al., 2003; Spergel et al., 2003) should amount to $\Omega_b = (4.6 \pm 0.2)$ % of the total cosmological mass/energy density $\Omega_b + \Omega_{DM} + \Omega_{DE}$. While this number is in good agreement with the number of baryons 'counted' in the HI Ly α Forest at $z > 2$, $\Omega_b > 3.5$ % (Rauch, 1998; Weinberg et al., 1997), a large discrepancy is found in the Local Universe, at $z < 2$. The total number of baryons seen at low redshift in virialized matter (i.e. stars, neutral H and He, molecular H, and X-ray emitting plasma in clusters of galaxies: Fukugita, 2003) and not yet virialized matter (residual HI Ly α Forest - Penton, Stocke & Shull, 2004 -, and both photoionized and collisionally ionized OVI in the Intergalactic Medium - Tripp, Savage & Jenkins, 2000; Savage et al., 2002) amount to only $\Omega_b(z < 2) = (2.5 \pm 0.3)$ %. About 46 % of the total predicted baryons are then missing at $z < 2$: $\Omega_b(\text{missing}) = (2.1^{+0.5}_{-0.4})$ % (Nicastro et al., 2004a - N04a -, and references therein).

Hydrodynamical simulations for the formation of large-scale structures in the Universe predict that these baryons hide in a filamentary web of tenuous ($n_b \simeq 10^{-6} - 5 \times 10^{-5} \text{ cm}^{-3}$, i.e. $\delta = n_b / \langle n_b \rangle \simeq 5 - 100$ ¹) matter at warm-hot temperatures ($T \simeq 10^5 - 10^7$ K) that permeates intergalactic space and connects already virialized structures (e.g. Hellsten, Gnedin & Miralda-Escudé, 1998; Cen & Ostriker, 1999; Davé et al., 2002; Fang, Bryan & Canizares, 2002). This primordial matter would provide the fuel for the assembly of galaxies and galaxy groups and clusters, and would be shock-heated during the continuous infall process of structure formation. The internal shocks ionizes the gas to such a degree that it becomes 'invisible' in infrared, optical or UV light, but should shine and absorb Far-UV and X-ray photons. However, given the very low-density, extremely high sensitivity, large-field of view, FUV or X-ray detectors are needed to image the emission from these filaments (e.g. Yoshikawa et al., 2003), and these are not yet available. The only avenue pursuable today, is to detect the WHIM in absorption against bright background sources.

Here we present two LETG spectra of the blazars Mrk 421 and 1ES 1028+511, and the first detections of three OVII WHIM filaments. A fourth filament is only detected in $CV_{1s \rightarrow 2p}$ in the 1ES 1028+511 spectrum. Sections 4 and 5 are devoted to the estimates of the number density and the cosmological mass density in the OVII WHIM, while in section 6 we discuss future prospects for WHIM studies. Throughout the paper we use LETG spectra grouped at a resolution of $\Delta\lambda = 12.5 \text{ m\AA}$ for fitting purposes, i.e. 4 times better than the intrinsic LETG resolution of 50 m\AA . The plots, instead, show spectra binned at 25 m\AA for Mrk 421 and 12.5 m\AA for 1ES 1028+511. Equivalent Width sensitivity limits are converted into ion column density limits by using Doppler parameters corresponding to thermal broadening of the lines in plasma at

¹ $\langle n_b \rangle = 2 \times 10^{-7} (1+z)^3 (\Omega_b h^2 / 0.02)$ is the average density in the Universe.

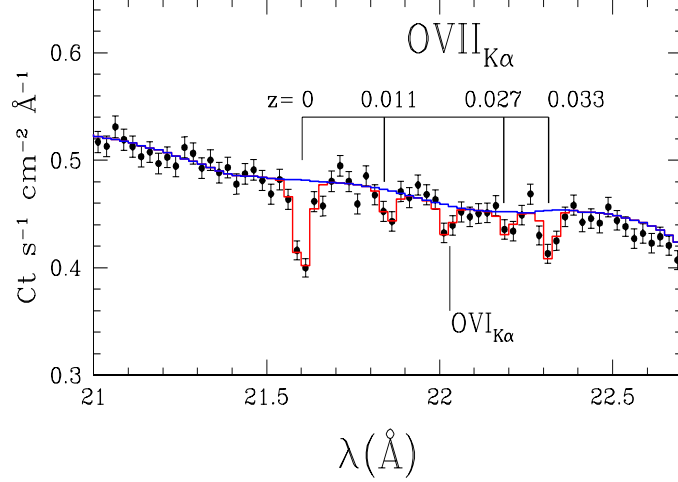


Fig. 1. 21-22.5 Å portion of the *Chandra*-LETG spectrum of Mrk 421. The dashed line shows the best fitting continuum, while the solid line is our best-fitting continuum plus line model.

$\log T(K) = 6.1$, the central temperature of the WHIM distribution (e.g. Davé et al., 2002). We adopt $H_0 = 72 \text{ km s}^{-1} \text{ Mpc}^{-1}$ (Freedman et al., 2001, Bennett et al., 2003). Errors are quoted at 1σ for 1 interesting parameter, unless otherwise stated.

2 LETG Spectra of Mrk 421 and 1ES 1028+511

Mrk 421 is a blazar at $z = 0.03$. We observed Mrk 421 with the *Chandra* LETG during two very luminous outbursts, on 2002, October, 26-27 and 2003, July 1-2, under our TOO programs to observe blazars in outburst phases. These two observations lasted ~ 100 ks each and caught the source at historical maxima, 60 and 40 mCrab in the 0.5-2 keV band, allowing us to collect a total of ~ 5300 Counts Per Resolution Element (CPREs) at 21 Å (Nicastro et al., 2004b: N04b). This S/N was enough to detect O VII columns of $N_{\text{O VII}} \gtrsim 8 \times 10^{14} \text{ cm}^{-2}$ at $\geq 3\sigma$. We detected 24 absorption lines in the LETG spectrum of Mrk 421, between 10 and 50 Å (see N04b for a full, detailed spectral analysis of both continuum and lines). While the majority of these lines are imprinted by both neutral and highly ionized systems at velocity consistent with zero (ISM gas, and either Local Group WHIM - Nicastro et al., 2002; Nicastro et al., 2003; Williams et al., 2004 - or an extended Galactic Corona - Sembach et al., 2003; Savage et al., 2004), 9 lines are instead identified with two intervening WHIM systems at $z = (0.011 \pm 0.001)$ and $z = (0.027 \pm 0.001)$. Figure 1 shows the 21-22.5 Å portion of the LETG spectrum of Mrk 421, in which the two $\text{OVII}_{1s \rightarrow 2p}$ lines from the two WHIM systems, together with the $z = 0$ lines of O VI and O VII (and possibly a fourth $\text{OVII}_{1s \rightarrow 2p}$ transition at $z = 0.033$, where also a $\text{HI Ly}\alpha$ is seen - Dull et al., 1996), are present.

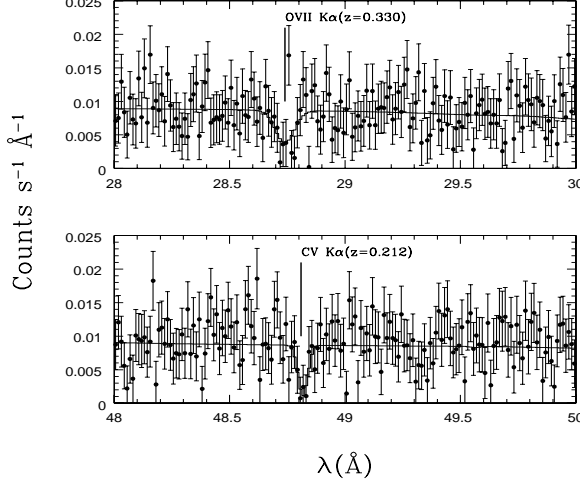


Fig. 2. Two portions of the HRC-LETG spectrum of 1ES 1028+511: (a) 28-30 Å and (b) 48-50 Å. The solid lines show our best fit models (the continuum is fitted over the broad range 10-60 Å). Two lines from O VII (top panel) and C V (bottom panel), from two intervening WHIM systems, are detected in these two portions of the 1ES 1028+511 spectrum.

1ES 1028+511 is a blazar at $z = 0.361$. It was observed under our *Chandra* TOO program, with the *Chandra* LETG, following a short outburst phase (3-days), on 2004, March 11. Although 1ES 1028+511 was back close to its 'quiescent' level when *Chandra* pointed at it, 1ES 1028+511 turned out to be a bright soft X-ray source for such a high redshift ($F_{0.5-2\text{keV}} = 1.1$ mCrab). The 150 ks HRC-LETG spectrum of 1ES 1028+511 contains 80-100 CPREs in the $21 < \lambda(\text{\AA}) \leq 50$ interval, enough to detect at 3σ $N_{\text{O VII}} \geq 1.4 \times 10^{16} (1+z)^{-2} \text{ cm}^{-2}$ at $z \leq 0.361$, and 4.1 times lower C V columns, $N_{\text{C V}} \geq 3.4 \times 10^{15} (1+z)^{-2} \text{ cm}^{-2}$ at $z \leq 0.269$ (at $\lambda > 51$ Å i.e. $z > 0.269$ for $\text{C V}_{1s \rightarrow 2p}$, the spectrum is heavily affected by the presence of the HRC plate gap). Although the analysis of these data is still in progress, we show here some preliminary results. We detect two strong lines (3.5σ and 4.4σ) at $\lambda = 28.740 \pm 0.038$ Å and $\lambda = 48.816 \pm 0.040$ Å that we identify as $\text{O VII}_{1s \rightarrow 2p}$ from a WHIM system at $z = 0.330 \pm 0.002$, and $\text{C V}_{1s \rightarrow 2p}$ from a WHIM system at $z = 0.212 \pm 0.001$ (Figure 2 (a) and (b) respectively; Nicastro et al., 2005, in preparation: N05). Errors on λ and z include a 20 mÅ (1σ) calibration uncertainty in the HRC-LETG dispersion relationship (see e.g. N04b and references therein). We also detect the N VII Ly α at the redshift of the O VII system ($z = 0.330$), but only at a significance of 2.6σ .

3 WHIM Solutions for the O VII Systems

For the two O VII-N VII absorbers along the line of sight to Mrk 421 (and also based on their measured H I and O VI upper limits, from HST-STIS and FUSE

Table 1

WHIM Solutions for the Three O VII Systems

Redshift	T (10^6 K)	N_b ^a	D ^b	[O/H]
(0.011 ± 0.001)	(0.6-2.5)	$(2.0 \pm 0.3)^c$	$(0.7 \pm 0.1)^c$	> -1.47
(0.027 ± 0.001)	(1.1-1.7)	$(2.8 \pm 0.2)^c$	$(0.9 \pm 0.1)^c$	> -1.32
(0.330 ± 0.002)	(1.6-2.5)	$(24 \pm 8)^d$	$(7.8 \pm 2.5)^d$	N/A

^a In units of $10^{19} 10^{-[O/H]-1} \text{ cm}^{-2}$. ^b In units of $10^{-[O/H]-1} (n_{b-5})^{-1} \text{ Mpc}$: (n_{b-5}) is the baryon density in units of 10^{-5} cm^{-3} . ^c At $\log T = 6.1$. ^d At $\log T = 6.3$.

respectively - N04b) we find self-consistent ionization balance and metallicity solution, that allow us to derive equivalent H column density and temperature range (N04a, N04b). These solutions are found by comparing the data with hybrid models of tenuous (i.e. $n_e \lesssim 10^{-4} \text{ cm}^{-3}$) collisionally ionized gas, undergoing the additional contribution of photoionization by the diffuse extragalactic UV-X-ray background (plus the proximity effect of the beamed radiation from the blazar, in the case of the line of sight to Mrk 421: see N04b for details). From these solutions, and assuming homogeneity in the systems (which may not be appropriate, given the evidence for the co-existence of multi-phase structures for at least one of the two filaments: N04b), we derive the depth of these filaments along our line of sight, in terms of the baryon volume density in units of $n_b = 10^{-5} \text{ cm}^{-3}$. The first two rows of table 1 summarize the results.

For the two O VII/CV systems along the line of sight to 1ES 1028+511, our analysis is still in progress. Table 1 (3rd row) contains only rough estimates of the equivalent H column density, temperature and depth of the O VII filament, derived based on the $N_{\text{O VII}}$, $N_{\text{N VII}}$ measurements and the $N_{\text{O VIII}}$ 3σ upper limit. Metallicity estimates for this object are currently not available.

4 Number Density of O VII WHIM Filaments

Figure 4 shows the predicted cumulative number of O VII WHIM system per unit redshift as a function of the minimum O VII column density (solid curve; Fang, Bryan & Canizares, 2002). The lowest O VII column density we detect along the line of sight to Mrk 421, is $N_{\text{O VII}} = 7 \times 10^{14} \text{ cm}^{-2}$, which is about the 3σ sensitivity of the spectrum of Mrk 421 in the entire $z \leq 0.03$ redshift range. The redshift of 1ES 1028+511, instead, is much higher, so we cannot neglect the dependence of the $N_{\text{O VII}}$ detection sensitivity threshold on the wavelength (see §6). The LETG spectrum of 1ES 1028+511 has a $> 3\sigma$ -sensitivity to $N_{\text{O VII}} = 8.7 \times 10^{15} \text{ cm}^{-2}$ (the column of the detected O VII line at $\lambda = 28.74$) for $0.269 \leq z \leq 0.361$, a redshift interval of $\Delta z = 0.092$. At $z < 0.269$ the

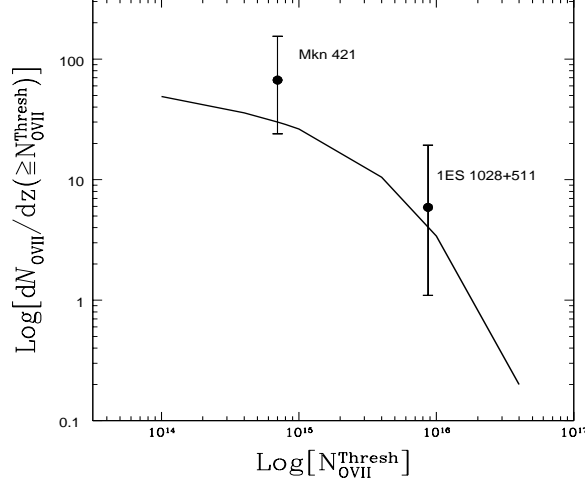


Fig. 3. Predicted cumulative number of O VII WHIM systems per unit redshift as a function of the minimum O VII column density (solid curve; Fang, Bryan & Canizares, 2002). The two points are the cumulative numbers of $> 3\sigma$ detected O VII WHIM filaments per unit redshifts, down to $N_{\text{OVII}}^{\text{Thres}} = 7 \times 10^{14} \text{ cm}^{-2}$ (line of sight to Mrk 421) and $N_{\text{OVII}}^{\text{Thres}} = 8.7 \times 10^{15} \text{ cm}^{-2}$ (line of sight to 1ES 1028+511).

effective redshift range within which we can detect $N_{\text{OVII}} \geq 8.7 \times 10^{15} \text{ cm}^{-2}$ at a significance $> 3\sigma$ is $\Delta z_{\text{eff}} = 0.075$ (see N05 for details). So, the total effective redshift range is $\Delta z_{\text{tot}} = \Delta z_{\text{eff}} + \Delta z = 0.167$.

The cumulative numbers of $> 3\sigma$ detected O VII WHIM filaments per unit redshifts, down to $N_{\text{OVII}}^{\text{Thres}} = 7 \times 10^{14} \text{ cm}^{-2}$ and $N_{\text{OVII}}^{\text{Thres}} = 8.7 \times 10^{15} \text{ cm}^{-2}$, are therefore: $d\mathcal{N}/dz(> 7 \times 10^{14}) = 70_{-40}^{+90}$ and $d\mathcal{N}/dz(> 8.7 \times 10^{15}) = 6_{-5}^{+13}$ (Fig. 3; the large errors are due to the small number statistics: Gehrels, 1986). At 1.4σ the two points are inconsistent with a constant value. The best fit slope of the power law connecting the two points is $\alpha = 1.0_{-0.7}^{+0.5}$. The solid line in Figure 3 shows that the model predictions of [14] are consistent (within the large errors) in both normalization and slope with the observations.

5 Cosmological Mass Density of O VII WHIM Filaments

Based on the equivalent H column density measurements from three O VII WHIM filaments (Table 1), we can now estimate the baryonic cosmological mass densities Ω_b^{WHIM} down to our two values of $N_{\text{OVII}}^{\text{Thres}}$. We obtain $\Omega_b^{\text{WHIM}}(> 7 \times 10^{14}) = (2.7_{-0.9}^{+3.8}) \times 10^{-[O/H]-1} \%$ (N04a) and $\Omega_b^{\text{WHIM}}(> 8.7 \times 10^{15}) = (2.0_{-1.8}^{+4.7}) \times 10^{-[O/H]-1} \%$ (N05), for the lines of sight to Mrk 421 and 1ES 1028+511 respectively. Errors on these estimates include the (dominant) asymmetric Poisson errors associated with a small number of events (Gehrels, 1986). One can try to reduce these errors combining the two Ω_b^{WHIM} measurements. However, to do this, we have to extrapolate the 1ES 1028+511 measurement, down

to the sensitivity of the Mrk 421 spectrum, i.e. down to $N_{\text{O VII}} = 7 \times 10^{14} \text{ cm}^{-2}$. First of all we have to derive an equivalent redshift range Δz_{eq} , within which we would expect to detect a single O VII WHIM filament with $N_{\text{O VII}} = 7 \times 10^{14} \text{ cm}^{-2}$ along the line of sight to 1ES 1028+511. We obtain $\Delta z_{\text{eq}} = 0.023$ (see N05 for details). From Δz_{eq} we can derive an equivalent $d_{\text{eq}}^{\text{1ES}}$ distance to 1ES 1028+511 that we will use in the formula for Ω_b . Next we need to evaluate the probability P that this single O VII filament has $N_{\text{O VII}} \geq 8.7 \times 10^{15} \text{ cm}^{-2}$, and use it in the formula for Ω_b to weight the $N_{\text{H}}^{\text{1ES}}$ measurement (Table 1). We find $P \simeq 0.14$ (see N05 for details). This gives a combined Ω_b estimate $\Omega_b^{\text{WHIM}}(\geq 7 \times 10^{14}) = (2.4_{-1.1}^{+1.9}) \times 10^{-[O/H]^{-1}} \%$, consistent with both model predictions and the actual number of missing baryons.

6 WHIM Detectability

The WHIM imprints high-ionization metal absorption lines, both in the FUV (mainly O VI) and in the X-rays (transitions from He-like and H-like C, N, O and Ne, and inner shell transitions from lower ionization ions). While high signal-to-noise FUSE FUV spectra of tens of low-redshift AGNs are readily available, the observed number density of relatively cool ($T \simeq 10^5 - 10^{5.5} \text{ K}$) shock-heated O VI filaments with $N_{\text{O VI}} \geq 4 \times 10^{13} \text{ cm}^{-2}$ (the average threshold sensitivity of high signal to noise FUSE spectra of AGNs) is low: $d\mathcal{N}/dz = 14_{-6}^{+9}$ (Savage et al., 2002). The predicted number density of the hotter ($T \simeq 10^{5.5} - 10^{6.5}$) O VII-dominated filaments, down to the same columns ($N_{\text{O VII}} \geq 4 \times 10^{13} \text{ cm}^{-2}$), is a factor of 5 larger, and decreases to that observed for O VI at column densities ~ 2 orders of magnitude larger ($N_{\text{O VII}} \geq 4 \times 10^{15} \text{ cm}^{-2}$: Fig. 3). The total equivalent H column density (and so the baryon mass) implied by 'pure' O VII filaments (i.e. systems in which the O VI columns are below the current sensitivity threshold) is then more than one order of magnitude larger than that of 'pure' O VI filaments: the bulk of the WHIM can only be detected in the X-ray band. Detecting He-like absorption lines with $N_{\text{ion}} \leq 2 \times 10^{15}$ at $\lambda = 22 \text{ \AA}$ (about the restframe wavelength of O VII_{1s→2p}) at the spectral resolution of the current X-ray spectrometers ($\Delta\lambda = 50 \text{ m\AA}$ for both the *Chandra* Low Energy Transmission Grating - LETG - and the XMM-*Newton* Reflection Grating Spectrometer - RGS), requires X-ray spectra with ≥ 600 CPREs in the continuum (Fig. 4, solid line). This requirement relaxes significantly at longer wavelength, since $N_{\text{ion}}^{\text{Thres}}$ (for given grating resolution and CPREs) decreases with λ^{-2} . So, for example, at $\lambda = 47 \text{ \AA}$ ($z = 1.18$ for the O VII_{1s→2p}, but only $z = 0.16$ for the C V_{1s→2p}) only ~ 120 CPREs are required to reach the same 3σ sensitivity of $N_{\text{ion}} \leq 2 \times 10^{15}$ (Fig. 4, dashed line). Unfortunately, however, the highest quality LETG or RGS spectra of the brightest (and very nearby) AGNs contains at most 50 CPREs. Two important exceptions are the cases presented here: the LETG spectra of the two blazars

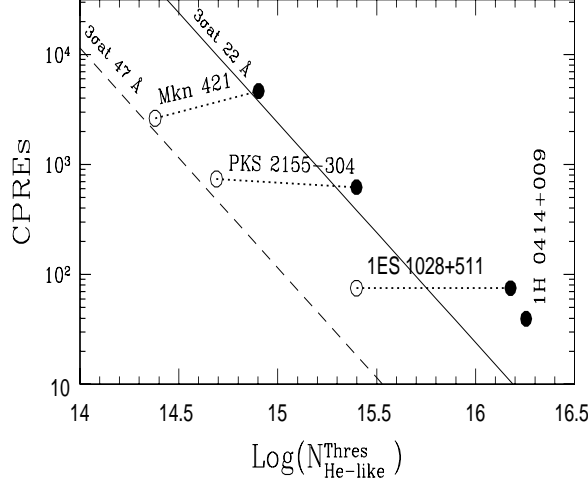


Fig. 4. CPREs as a function of $3\sigma N_{\text{He-like}}^{\text{Thres}}$ (we use the oscillator strength of the $\text{O VII}_{1s \rightarrow 2p}$, $f = 0.696$). The solid and dashed lines are the approximate analytical relation $N_{\text{He-like}}^{\text{Thres}} \simeq 1.1 \times 10^{17} N_{\sigma} (\Delta\lambda(\text{m}\text{\AA})) (\text{CPREs})^{-1/2} \lambda(\text{\AA})^{-2}$, at 22 \AA and 47 \AA , respectively. In this formula columns are in cm^{-2} , N_{σ} is the number of σ (3 in the plotted curves), $\Delta\lambda$ is the grating resolution in $\text{m}\text{\AA}$ (50 $\text{m}\text{\AA}$ for both curves). Data points are the measured $3\sigma N_{\text{He-like}}^{\text{Thres}}$ upper limits at 22 \AA (filled circles) and at 47 \AA (empty circles) from the *Chandra* spectra of Mrk 421, PKS 2155-304 and 1ES 1028+511 and the XMM-Newton spectrum of 1H 0414+009. These empirical data nicely confirm the analytical curves for $\text{CPRE} \gtrsim 100$. At lower CPREs data deviate from the ideal analytical curves, due to deviations of the actual signal-to-noise ratio in the data from the ideal Poissonian $\sqrt{\text{CPREs}}$. We note that about 80 CPREs are needed for a 3σ detection of $N_{\text{He-like}} = 1.5 \times 10^{16} \text{ cm}^{-2}$ at 22 \AA (1ES 1028+511, filled circle), but about 6 times lower columns are 3σ -detectable with the same number of CPRE, at 47 \AA (1ES 1028+511, empty circle).

Mrk 421 ($z = 0.03$) and 1ES 1028+511 ($z = 0.361$), observed by *Chandra* under our TOO programs, while undergoing outbursts.

7 Future Prospects

This work only begins the study of the Warm-Hot IGM outside the Local group (Nicastro et al., 2002, 2003; Williams et al., 2004), now that the WHIM has been detected and theoretical predictions have been verified.

The large number of ion species showing up in the X-ray spectra imply a rich field of investigation. Higher significance detections, along several other lines of sight, and at higher redshift, of He-like and H-like transitions from C, N, O and Ne, will allow us to measure the relative metallicity ratios at different redshifts. This will fundamentally contribute to the assessment of the still poor measurements of metal production with cosmic age, and will help refining mechanisms for galaxy/AGN-IGM feedback (e.g. galaxy superwinds, quasar

winds). Moreover, the potential for the simultaneous detection, in the same band, of inner-shell transition from lower ionization species of the same ions, will allow us to distinguish between different ionization scenarios, and to assess the importance and frequency of multiphase IGM. Spectral resolutions of $R \geq 3000$ in the soft X-ray band will allow us to separate different kinematics components. This has already been proven very useful in the FUV band, for example to distinguish between a Local Group WHIM origin and a halo origin for the O VI high-velocity absorbers at $z \simeq 0$ (Nicastro et al., 2003). Reconstructing the distribution functions of several ions in the WHIM (i.e. $dN/dz dN$), will also prove very useful in distinguishing different cosmologies, and possibly tracing the distribution of dark-matter potential wells in the local Universe.

Observing sources with *Chandra* while in bright outburst phases has proven fruitful, allowing the detection of the WHIM for the first time. However, Mrk 421 is unique: no other extragalactic sources in the sky (except Gamma-Ray Burst X-ray afterglows, e.g. Fiore et al., 2000) reach the level of Mrk 421 during the observations presented here. While relatively short *Chandra* and/or XMM-*Newton* observations of blazars in outburst will continue to provide a 'cheap' way to probe new sightlines for WHIM studies, substantial progresses in our understanding of the WHIM phenomenon can only be made by exploiting different observational strategies.

As shown in Fig. 3, the expected number of O VII WHIM filaments down to a given $N_{\text{O VII}}$ threshold, increases linearly with redshift. About 2 O VII filaments with $N_{\text{O VII}} \geq 10^{16}$ are expected up to $z = 0.5$ along a random line of sight. Such O VII columns can easily be detected with 100 ks *Chandra* and/or *Newton*-XMM observations of background sources flaring at a level even 10 times lower than that reached by Mrk 421 during the observations presented here.

An important metric for future instrumentation to explore the WHIM, as shown in figure 4, is that the sensitivity of a grating spectrum (i.e. $\Delta\lambda = \text{const}$) with constant signal to noise per resolution element, to a given column density, increases rapidly with redshift ($\propto (1+z)^2$). Smaller columns are detectable at higher redshift, as beautifully proven by the faint C V_{1s→2p} detection in the moderate signal-to-noise *Chandra* spectrum of 1ES 1028+511 (about 60 times fainter flux than the *Chandra* Mrk 421 observations presented here: Fig. 2b). These are key elements for planning future observational strategies and mission designs for WHIM studies. Long integrations, $\gtrsim 0.5 - 1$ Ms, with *Chandra* and/or XMM-*Newton* of high- z sources in their quiescent states are low-risk and possibly the only way to dramatically increase the number of detections and so narrow down the large statistical errors on the Ω_b^{WHIM} estimate. Tripling the currently detected number of WHIM systems, by exploiting the above observational strategy, is within the reach of current X-ray instruments, and

will allow us to reduce the uncertainties on Ω_b^{WHIM} down to \sim_{-40}^{+60} %, the level to which the other baryonic components in the local Universe are now known (e.g. N04a and reference therein).

Further advances in this direction will have to wait for the large collecting area of the spectrometers on the two planned X-ray missions, *Constellation-X*² and *XEUS*³ or dedicated small missions, e.g. *Pharos* (Elvis et al., 2002). With ~ 100 times larger effective area and $R > 1000$, *Constellation-X* will allow us to detect WHIM systems as weak as those presented in this work, for dozens of different lines of sight, and thicker filaments will be detected towards hundreds of different sightlines.

This will be much more effectively done with gratings than calorimeters, particularly if the currently undergoing tests on the off-plane reflection gratings configuration for *Constellation-X* will confirm the recently reached first-order peak absolute efficiency of 43 % (Heilmann et al., 2004)⁴. In calorimeters the resolution is constant in energy, and so the resolution element in $\Delta\lambda$ degrades as $\propto \lambda^2$. This dependence exactly cancels out the increase in N_{ion} sensitivity given by the formula $N_{\text{ion}}^{\text{Thres}} \gtrsim (\Delta\lambda)\lambda^{-2}$, at $\Delta\lambda = \text{const}$ (Fig. 4). Moreover, the degradation of calorimeter resolution with wavelength would greatly hamper the possibility of resolving WHIM lines (expected at $\lambda > 20$ Å) or detecting multiphase structures in the IGM (and so prevent tests of the current paradigms for the dominant heating mechanism: internal shocks). This would in turn hamper our capabilities of tightly constrain the physical properties of the baryons in this diffuse web of WHIM.

A resolving power $R \gtrsim 5000$ is needed to resolve thermally broadened O lines in gas at $T = 10^6$ K and so to allow for separation of different components, and for a clear physical diagnostics (Elvis et al., 2002), which may be achievable with *Constellation-X* or *Pharos*.

Finally we note that it is crucial that the intrinsic noise of the detector containing the dispersed spectrum be extremely low. Figure 4 shows that the lowest CPRE point, from the RGS observation of 1H 0414+009, is actually closer to the ideal analytical sensitivity curve, CPREs vs $N_{\text{He-like}}^{\text{Thres}}$, than the one from the HRC-LETG observation of 1ES 1028+511. The HRC-LETG spectrum of 1ES 1028+511 has almost twice as many CPRE as the RGS spectrum of 1H 0414+009, but a 5 times larger intrinsic instrumental noise (5.2×10^{-5} cts s⁻¹ per resolution element), which greatly penalizes the detection of faint columns. High resolving-power/efficiency X-ray gratings dispersed onto low-noise detectors are therefore, by far, the most efficient instruments to systematically study the WHIM in the near future.

² <http://constellation.gsfc.nasa.gov/science/index.html>

³ <http://www.rssd.esa.int/index.php?project=XEUS>

⁴ snl.mit.edu/papers/papers/2003/Heilmann/RKH-SPIE-5168.pdf

References

- [1] Bennet, C.L. et al., First Year Wilkinson Microwave Anisotropy Probe (WMAP) Observations: Preliminary Maps and Basic Results, *ApJS*, 148, 97-117 (2003)
- [2] Cen, R. & Ostriker, J.P., Where are the Baryons?, *ApJ*, 514, 1-6 (1999)
- [3] Davé, R. et al., Baryons in the Warm-Hot Intergalactic Medium, *ApJ*, 564, 604-623 (2002)
- [4] Elvis, M., Fiore, F. & the Pharos Team, A High Resolution Intergalactic Explorer for the Soft X-ray/FUV, SPIE (August 2002), astro-ph/0303444 (2003)
- [5] Fang, T., Bryan, G.L. & Canizares, C.R., Simulating the X-ray Forest, *ApJ*, 564, 604-623 (2002)
- [6] Fiore, F., et al., Probing the Warm Intergalactic Medium through Absorption against Gamma-Ray Burst X-Ray Afterglows, *ApJ*, 544, L7-L10 (2000)
- [7] Fukugita, M., Cosmic Matter Distribution: Cosmic Budget Revisited, to be published in the proceedings of IAU symposium 220, Dark Matter in Galaxies, astro-ph/0312517 (2003)
- [8] Gehrels, N., Confidence Limits for Small Numbers of Events in Astrophysical Data, *ApJ*, 303, 336-346 (1986)
- [9] Hellsten, U., Gnedin, N.Y. & Miralda-Escudé, J., The X-Ray Forest: A New Prediction of Hierarchical Structure Formation Models, *ApJ*, 509, 56-61 (1998)
- [10] Kirkman, D. et al., The Cosmological Baryon Density from the Deuterium-to-Hydrogen Ratio in QSO Absorption Systems: D/H toward Q1243+3047, *ApJS*, 149, 1-28 (2003)
- [11] Nicastro et al., A Warm-Hot Intergalactic Medium Location for the Missing Cosmic Baryons, *Nature*, accepted for publication (2004): N04a
- [12] Nicastro, F. et al., Chandra Detection of the First X-ray Forest along the Line of Sight To Mrk 421, *ApJ*, submitted (2004): N04b
- [13] Nicastro, F. et al., The Far Ultraviolet Signature of the 'Missing' Baryons in the Local Group of Galaxies, *Nature*, 421, 719-721 (2003)
- [14] Nicastro, F. et al., Chandra Discovery of a Tree in the X-ray Forest toward PKS 2155-304: The Local Filament?, *ApJ*, 573, 157-167 (2002)
- [15] Penton, S.V., Stocke, J.T. & Shull, J.M., The Local Ly α Forest. IV. Space Telescope Imaging Spectrograph G140M Spectra and Results on the Distribution and Baryon Content of H I Absorbers, *ApJS*, 152, 29-62 (2004)
- [16] Rauch, M., The Lyman Alpha Forest in the Spectra of QSOs, *ARA&A*, 36, 267-316 (1998)

- [17] Savage, B.D. et al., Far Ultraviolet Spectroscopic Explorer and Space Telescope Imaging Spectrograph Observations of Intervening O VI Absorption Line Systems in the Spectrum of PG 0953+415, *ApJ*, 564, 631-649 (2002)
- [18] Sembach, K.R. et al., Highly Ionized High-Velocity Gas in the Vicinity of the Galaxy, *ApJS*, 146, 165-208 (2003)
- [19] Spergel, D.N. et al., First Year Wilkinson Microwave Anisotropy Probe (WMAP) Observations: Determination of Cosmological Parameters, *ApJS*, 148, 175-194 (2003)
- [20] Tripp, T.M., Savage, B.D. & Jenkins, E.B., Intervening O VI Quasar Absorption Systems at Low Redshift: a Significant Baryon Reservoir, *ApJ*, 534, L1-L5 (2000)
- [21] Weinberg, D.H. et al., Lower Bound on the Cosmic Baryon Density, *ApJ*, 490, 564-570 (1997)
- [22] Yoshikawa, K., et al., Detectability of the Warm/Hot Intergalactic Medium through Emission Lines of O VII and O VIII, *PASJ*, 55, 879-890 (2003)